Tunable Nanowrinkles on Shape Memory Polymer Sheets

By *Chi-Cheng Fu, Anthony Grimes, Maureen Long, Christopher G. L. Ferri, Brent D. Rich, Somnath Ghosh, Sayantani Ghosh, Luke P. Lee, Ajay Gopinathan,* and *Michelle Khine**

Researchers have long been fascinated by wrinkles as a pervasive natural phenomenon.[1–4] Recently, there has been a resurgence of interest in emulating and leveraging wrinkles for various applications. Polymeric wrinkles are finding increased utility as complex quasiperiodic structures important in applications, including cell-fate studies.[5,6] Flexible integrated circuits promising many new applications, such as wearable systems, have been demonstrated using thin buckled films of single-crystalline silicon based on elastomeric substrates.[7,8] Metal wrinkles, thin films of metal on polymer substrates, have promise for applications in molecular detection, optical devices, filters and sorters, high-surface-area conductors and actuators, and even metrology.[9–12] We have developed a rapid approach to create metal nanowrinkles of tunable size and demonstrable utility on a shape memory polymer,[13,14] pre-stressed polystyrene (PS) sheets commercially available as the children's toy Shrinky-Dinks.

Previous demonstrations of wrinkles exhibited relatively large wrinkle wavelengths. For instance, Bowden et al. deposited metal onto a thermally expanded polydimethylsiloxane (PDMS) polymer; the cooling of the PDMS causes a compressive stress, which buckles the deposited metal film to achieve ca. 30 µm structures.[9] Huck et al. augmented this approach with photochemically patterned areas that differ in stiffness and thermal expansion.[15] Watanabe and Hirai more recently developed the very simple approach of simply pre-stretching the PDMS sheet to achieve 6–20 µm striped patterns.[16] Lacour et al. used this approach to create stretchable gold conductors.[11]

[*] Prof. M. Khine
Department of Biomedical Engineering
University of California, Irvine
Irvine, CA 92697 (USA)
E-mail: mkhine@uci.edu
C.-C. Fu, A. Grimes, M. Long, B. D. Rich
School of Engineering
University of California, Merced
Merced, CA 95344 (USA)
C. G. L. Ferri, S. N. Ghosh, Prof. S. Ghosh, Prof. A. Gopinathan
School of Natural Sciences
University of California, Merced
Merced, CA 95344 (USA)
Prof. L. P. Lee
Department of Bioengineering
University of California, Berkeley
Berkeley, CA 94720 (USA)

Yoo et al. imposed order on the buckling of polystyrene by applying a physical mold during the buckling process.[17] While this group was able to achieve higher resolution wrinkles than previously reported (down to 2 µm periodicity) as well as directionality, the process required a microfabricated mold and took several hours.

Here, by just leveraging the stiffness mismatch of materials, we present a simple and ultra-rapid two-step (metal deposition and subsequent heating) method to controllably create nanometer-scale metal wrinkles. First, a 10 nm thick gold film is deposited on the PS sheets. Heating at 160 °C causes the substrates to retract to less than half of its original size and therefore induces the stiffer, nonshrinkable metal film to buckle (Fig. 1a, left).[18–20] Scanning electron microscopy (SEM) images (Figs. 1b and 2a) show that large areas of uniform biaxial nanowrinkles can be produced. To determine the resulting wrinkle wavelengths, we took the two-dimensional fast Fourier transform (2D FFT, shown in the inset of Fig. 2a) of the SEM images. The resulting disc-shaped power spectral densities indicate a broad distribution of wrinkle wavelength in *k*-space. From this, we can determine the distribution of wavelengths as a probability function. As shown by the black line in Figure 2b, the prevailing wavelengths peak near 400 nm and range from ca. 200 nm to ca. 1 µm. This range is smaller but more heterogeneous than those reported from other approaches, where the wrinkles had periodicities ranging from 20 µm to 50 µm.[9] As discussed below, we can adjust this broader range to our advantage for sensing applications.

In order to tune the wavelength of the wrinkles, it is important to understand how the length scales of the wrinkles depends on the thickness of the metal film, the material properties of the film and substrate, and the overall shrinking strain produced. Wrinkles arise from competition between the elastic bending energy of a stiff skin and the elastic energy of deformation of the soft substrate on which it is supported.[2,3,21] For a skin of thickness h and Young's modulus Y_{skin} supported on a substrate of Young's modulus Y_{sub}, minimization of the overall elastic energy yields an equilibrium wrinkle wavelength of $\lambda \propto \eta^{1/3}h$, where $\eta \propto Y_{skin}/Y_{sub}$.[2,3,21] For large compressive stresses, it is known that hierarchical wrinkling can occur because the amplitude of the smaller, first generation wrinkles saturate, forming an effective skin that can undergo a similar wrinkling process with wavelengths $\lambda \propto \eta_{eff}^{1/3}h_{eff}$, where η_{eff} and h_{eff} are the parameters corresponding to the new effective skin.[1] For biaxial strains, another critical length scale is the distance ξ, over which

Final page numbers not assigned

WILEY InterScience®
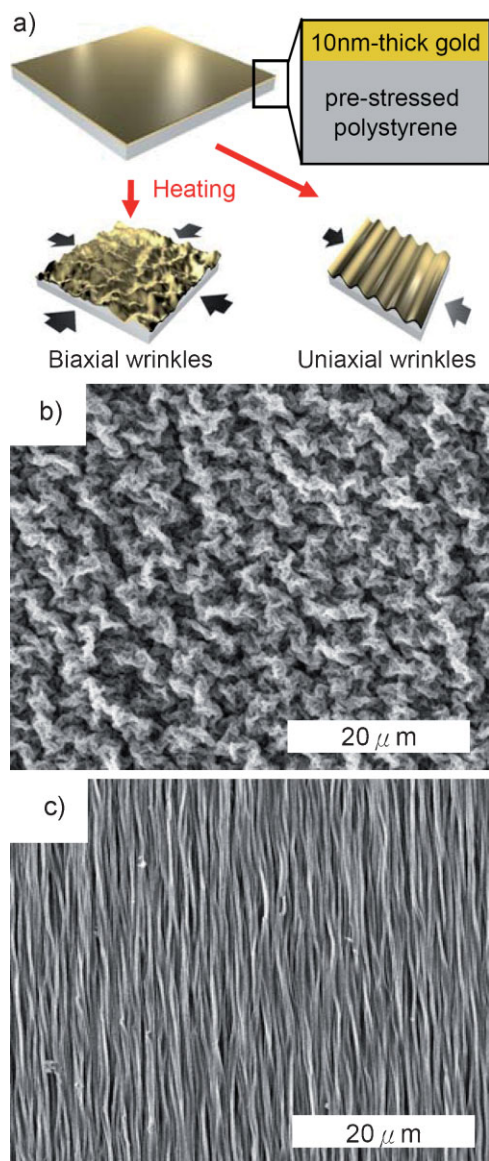DISCOVER SOMETHING GREAT

Figure 1. Fabrication of nanowrinkles. a) Scheme of fabrication of biaxial (left) and uniaxial (right) wrinkles. b,c) SEM images of biaxial (b) and uniaxial (c) wrinkles on shrunk polystyrene sheets covered with a 10 nm thick layer of gold.

Figure 2. Characterization of nanowrinkles. a) SEM image of biaxial wrinkles with 10 nm thick gold. Inset: Its 2D FFT pattern. b) Wavelength distributions of biaxial wrinkles with various thickness of gold. c) Main panel: SEM image of uniaxial wrinkles with 10 nm thick gold. Inset: Its 2D FFT pattern. Bottom panel: Cross-sectional SEM view. d) Wavelength distributions of uniaxial wrinkles with various thickness of gold. e) Plot of main wavelength of biaxial (black triangles) and uniaxial (red circles and blue squares) wrinkles as a function of gold layer thickness. The dashed lines show anticipated slopes from the theory. Note that ''1'' and ''2'' in (c), (d), and (e) indicate the first and the second populations of uniaxial wrinkle wavelengths.

wrinkles lose orientational coherence. It scales as $\xi \propto \eta^{2/3} h$.[22] For our case, a gold film ($Y_{gold} \approx 78$ GPa) on a PS substrate ($Y_{PS} \approx 3.5$ GPa), we anticipate $\eta = Y_{gold}/Y_{PS} \approx 22.3$.[23,24]

To verify the theoretical predictions, we varied the thickness of deposited gold from 10 nm to 50 nm. This caused a shift of hundreds of nanometers in the wavelength distributions (Fig. 2b). The experimental scaling of the peak wavelength with film thickness (the black triangles of Fig. 2e) has a slope of 8.4, which agrees well with our theorized slope for the scaling of the coherence length $\eta^{2/3} \approx 7.9$ (the black dashed line of Fig. 2e). This suggests that a loss of coherence is the dominant effect in determining the morphology in the biaxial case. It should be noted, however, that there is an offset, indicating a modified skin approximately 30 nm thicker than the bare metal film and with a
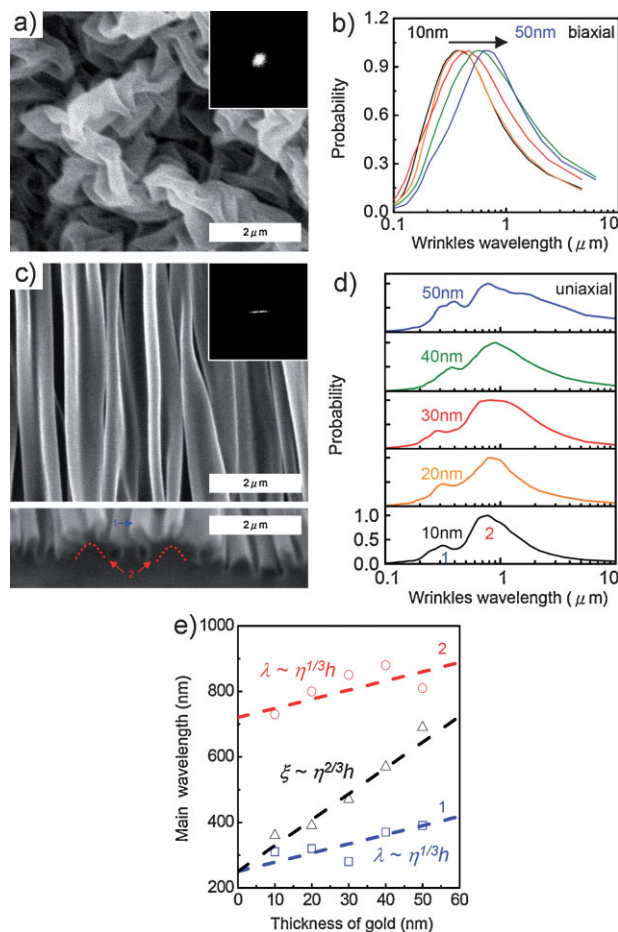
comparable modulus. The occurrence of such modified films has been reported previously[9] and is a likely consequence of the penetration of the metal into the substrate during the heat-shrinking process. Heating at 160 °C, above the glass transition temperature (95 °C) and below the melting temperature (240 °C) of PS, induces the substrate to become soft enough to be integrated into the wrinkling metal.[24] This phenomenon dramatically increases the binding strength between gold and PS and thus changes the durability of the wrinkles, as confirmed by our empirical measurements and SEM analyses. Compared with a flat gold film (film deposited after shrinking process but heated), which can be easily removed, wrinkles are considerably stronger and can even bear ultrasonic cleaning over 5 min (data not shown).

2

© 2009 WILEY-VCH Verlag GmbH & Co. KGaA, Weinheim

Adv. Mater. **2009**, 21, 1–5

Final page numbers not assigned

Uniaxial wrinkles can be easily created as well (Fig. 1a, right). We modify the fabrication process by introducing boundary conditions by clamping two edges of a gold-coated PS sheet during the heating process. This gives rise to constrained shrinking along one direction. Large areas of well-aligned linear wrinkles can be produced (Fig. 1c). For the 10 nm thick sample, these wrinkles exhibit two distinct populations with peaks at 300 nm and 800 nm (Figs. 2c,d). Their cross-sectional SEM image (Fig. 2c, bottom) demonstrates that the two populations correspond to two hierarchical generations of wrinkles.[9] Similar to what we found for the biaxial case, the peak wavelengths of both populations are proportional to the thickness of deposited gold and can thus be controllably tuned by adjusting the thickness of deposited gold (Fig. 2d). The scaling of the dominant wavelengths with film thickness for both first and second generations is linear, with slopes of 2.1 and 2.4, respectively (blue squares and red circles of Fig. 2e). The consistency between experimental results and the anticipated value for the bare metal film ($\eta^{1/3} \approx 2.8$, blue and red dashed lines in Fig. 2e) indicates that the loss of coherence is not the dominant issue, allowing us to clearly see features of the underlying wrinkle distribution. Thus, the first population (smaller wrinkles) can be regarded as arising from a modified skin of Young's modulus comparable to the bare metal but with a thickness about 130 nm greater than the metal film. As shown in the bottom panel of Figure 2c, the second population (larger wrinkles) arises from the saturation of the previous generation of wrinkles (first population), leading to the formation of an effective skin, which can still be regarded as having a modulus comparable to the bare metal but with a thickness that is about 300 nm greater than the metal film thickness. Since hierarchical wrinkling is a nonlinear process, it is difficult a priori to predict the effective skin thicknesses of successive generations. As a rough approximation, one can take the wrinkle amplitude (ca. $\Delta^{1/2}\lambda$, for overall strain Δ) of one generation to be the effective skin thickness for the next generation. The effective thicknesses for the first and second populations above are then consistent with second- and third-generation wrinkles for an overall strain of order unity.

We can also estimate an upper bound for the peak compressive stresses in the film if we assume all of the strain is relieved by the smallest wrinkles. This is an upper bound because some of the stress will be relieved by the higher order larger wrinkles. The stresses are then of the order of $Y_{gold}\Delta h/\lambda$, which yields values ranging from several hundred magapascals to 1 GPa over our range of thicknesses. While this is significantly larger than the yield point for bulk gold, it is known that the yield strength of materials at the nanometer scale shows a dramatic increase, of several orders of magnitude, compared to the bulk values.[25] For example, yield strengths of gold nanowires (3–6 GPa) are much greater than that of the bulk (55–200 MPa).[23] In particular, for metallic nanofilms on polymer substrates, most groups have found that the yield stress scales inversely with the film thickness, with the most recently measured yield stress value for a 50 nm gold film (which happens to be our highest film thickness) on PS substrates being as high as 30 GPa.[26] Thus, for the film thicknesses we use, our peak stresses are clearly well below the yield point — which means that predictions from linear elasticity theory are appropriate. This is further validated by the fact that

our experimental data agrees well with predictions using this simple theory.

Other metals, such as silver, can also be coated on PS sheets. Here we demonstrate that silver wrinkles can be fabricated and easily integrated into Shrinky-Dinks microfluidic-based devices, which were developed by our laboratory.[18–20] Besides the simple biaxial wrinkles (data not shown), uniaxial wrinkles can be aligned inside the microchannel. As shown in Figure 3a, first, a microchannel was patterned on a Shrinky-Dink sheet by manual scribing with a syringe tip. Second, we constrained it to shrink in only one direction, perpendicular to the direction of the channel. Third, a piece of channel-patterned adhesive tape was placed on its top as a mask during the silver-sputtering. Finally, after deposition of 40 nm thick silver, the tape was removed; heating without constraints makes the sheet shrink in the perpendicular direction and form uniaxial wrinkles. Figure 3b shows that these wrinkles are perpendicularly aligned within a channel with width of 280 µm. Thermal bonding can be achieved easily as described in our previous papers.[19,20]

Notably, our ability to achieve nanometer-scale wrinkles enables us to use these self-organized structures for surface plasmon resonance (SPR)-based sensing applications, such as metal-enhanced fluorescence (MEF). This technique utilizes metallic nanostructures in which the plasmons resonate with the fluorophores to reduce their excited state lifetimes and simultaneously increase their fluorescence emission intensities.[27] Silver island films are often used to meet such a requirement, and the typically ca. 10-fold enhancement has been applied to improve detection of DNA hybridization[28] and immunoassay.[29] However, detrimental chemical properties of silver, such as low stability and easy oxidization, inevitably restrict its potential in biomedical applications. Although the enhancement factor of gold is smaller, biocompatible gold in discrete nanostructures is, in contrast, free of these limitations and holds promise to enhance fluorescence intensity of fluorophores by a factor of ca. 2–7.[27,30] Recently, utilization of "continuous" gold nanometer-scale features to improve the density of hotspots has been studied; typically, a ca. 0.5- to 5-fold increase of the fluorescence intensity can be achieved.[31,32]

Here, we demonstrate that our continuous gold wrinkled substrate is useful for MEF as well. Figures 3c and d (top) show fluorescence images along with the corresponding intensity profiles of dyes, dissolved in polymer solution and then spin-coated on either a bare glass plate or uniaxial gold wrinkles.[33] The average fluorescence intensity increased approximately threefold over a relatively large area when the dyes were deposited on the wrinkles rather than the glass. Many bright lines parallel to the direction of the wrinkles indicates that there are many continuous hotspots along the wrinkles, with 5- to 7-fold enhancements. To confirm that the enhancement resulted from plasmon effects rather than aggregation of dyes, fluorescence lifetime measurements were performed with a homemade confocal microscope with a time-correlated single-photon counting module. Figure 3d (bottom) shows that the average fluorescence lifetime of dyes on a glass plate is 3.5 ns, but on wrinkles their average lifetime decreases dramatically to 0.4 ns (with a shorter lifetime of 0.3 ns and a longer lifetime of 1.7 ns). This ca. 9-fold decrease in average lifetime suggests that enhancement results from strong interactions between the
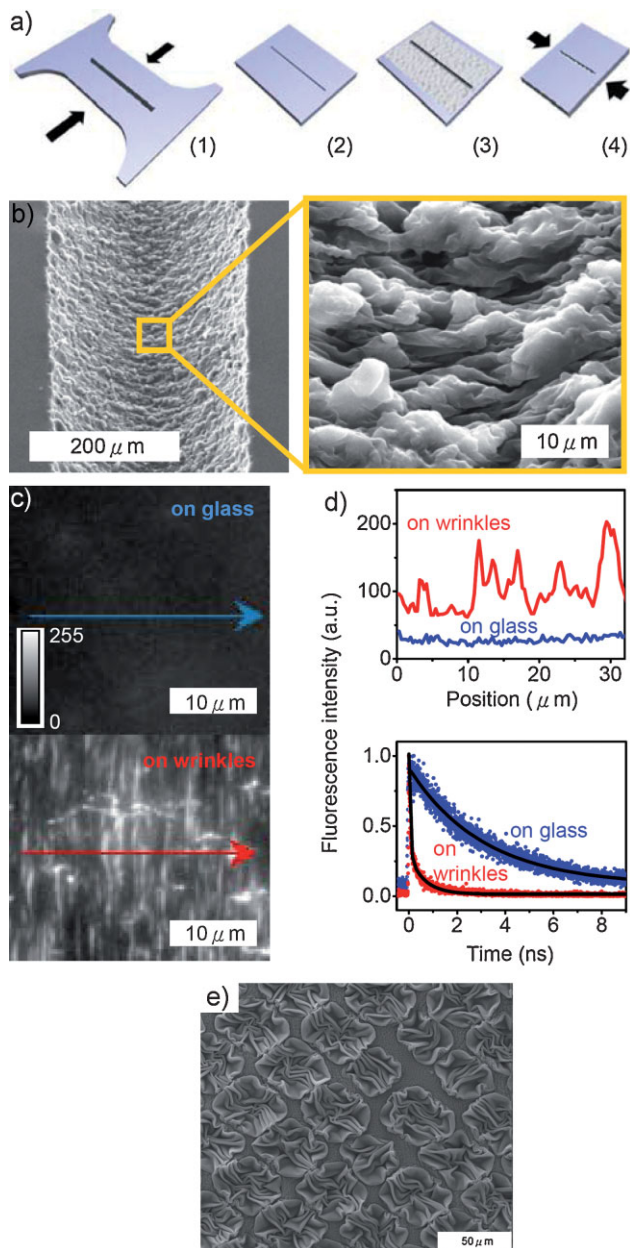
WILEY InterScience®
DISCOVER SOMETHING GREAT

Final page numbers not assigned

Figure 3. Utilities of nanowrinkles. a) Scheme of fabrication of uniaxial wrinkles inside a Shrinky-Dinks-based microchannel. b) SEM image of uniaxial wrinkles, with 45 nm thick silver layer, inside a channel. Right panel: Enlarged view of outlined area. c) Wide-field epifluorescence images of dyes on a glass plate (top) and on uniaxial wrinkles (bottom). d) Top: Fluorescence lifetime measurements of dyes on a glass plate (blue) and on wrinkles (red). The black lines show that each time trace can be well fitted with exponential decays. e) SEM image of discrete "wrinkled flowers".

fluorophore and surface plasmons.[27] In addition, the shorter and longer lifetimes may be attributed respectively to the strongly (bright) and weakly (dim) enhanced regions (Fig. 3c, bottom). Since the intensity of hotspots highly depends on the spacing between nanostructures, we suggest that the heterogeneous enhancement is correlated to the wavelength distribution of wrinkles.[34]

Compared with results from other continuous gold film nanostructures, a 7–fold enhancement is a significant achievement.[31,32] If the geometry of wrinkles is optimized, the critical spacing between the fluorophore and substrate controlled, and the density of intense hotspots increased, an average fluorescence intensity increase by at least one order of magnitude can be achieved. One potential MEF application is to improve the sensitivity of DNA and protein microarrays, in which high density probes with spot sizes from 10 to 500 μm are immobilized on substrates with areas of several square centimeters.[35] Fluorescence is widely adopted for detection owing to its ultrahigh sensitivity and capabilities for multiple-probe labeling. Recently, use of SPR to lower the detection limit has become desirable to broaden its applications.[35] To integrate our plasmonic material into commercial products, we demonstrated that our wrinkles can be easily patterned. In Figure 3e, discrete "wrinkled flowers" with diameters around 50 μm are shown to be well aligned. The sizes of spots and spaces depend on the resolution of the shadow mask and thus can be well controlled to be compatible with commercial detection systems.

In summary, our approach can create tunable nanowrinkles with broad yet tunable wavelength distributions. Such flexibility and heterogeneity hold a number of advantages over single, homogeneous, wavelength wrinkles. For instance, for further studies on multiple-probe MEF, these properties make it possible to adjust broad SPR bands to overlap well with various absorption bands of fluorophores.[27] In addition, our approach is considerably faster and significantly less expensive and more robust than other means of achieving such size-controllable nanometer-scale structures (including nanosphere lithography, focused ion beam lithography, and electron-beam lithography).[27] A significant enhancement of fluorescence intensity, together with the high throughput and fine microfluidic control over reagents with lab-on-chip techniques, makes the nanowrinkles promising low-cost substrates for ultrasensitive and ultrafast detection for biomedical applications.[36] In addition, such nanoscale features, along with ease of surface functionalization, make the gold wrinkles a potentially useful substrate for studying cell membrane dynamics.[37]

Experimental

Fabrication of Nanowrinkles and Discrete Wrinkled Flowers: For biaxial wrinkles, gold of varying nanometer thicknesses was deposited on a Shrinky-Dink sheet (or KSF50-C; Grafix, 2 cm × 1 cm) using sputtering (SEM coating system; Polaron). To avoid preheating of the substrate, this step was divided into four cycles, and each cycle (including 10 s of sputtering and 20 s of cooling) deposited 2.5 nm of gold. After deposition, heating at 160 °C for 6 min in an oven induced retraction of the substrate and caused the nonshrinkable gold film to form biaxial wrinkles. For uniaxial wrinkles, before heating two short edges of a gold-coated sheet were clamped by clips (2 inch (ca. 5 cm) binder clips; OfficeMax) to ensure it could only retract in the perpendicular direction. For discrete wrinkled flowers, the same approach was taken with the exception that an ad hoc shadow mask, a transmission electron microscopy (TEM) grid with 50 μm grid spacing, was placed over the PS sheet prior to sputtering. After sputtering, the physical shadow mask was simply removed and the patterned flowers left behind.

Integrating Wrinkles into Microchannels: First a Shrinky-Dink sheet (10 cm × 15 cm) was channel-patterned by manual scribing with a syringe

Final page numbers not assigned

tip (20 gauge luer stub syringe tip) to remove PS. Next, the sample is constrained by clips in one direction and allowed to shrink by heating it to 150 °C. After cooling, the center (2.5 cm × 5 cm) of the sample was cut out using a diamond saw. The chip was masked by placing adhesive tape (3M brand) on the surface of the sample adjacent to the channel previously scribed into the surface. The tape was aligned under a dissection microscope until the entire surface was covered and only the channel remained exposed. The sample was then coated with 45 nm of silver by sputter deposition. After coating, the tape was removed from the surface of the chip; what remained was only the silver that was deposited on the surface of the channel. The sample was then shrunk, without being constrained, at 150 °C to create uniaxial wrinkles inside the channel.

Materials and Methods for MEF Experiments: Dye molecules (Red CMTPX dyes, CellTracker; Invitrogen) with absorption peaking at 577 nm and emission peaking at 602 nm, were used. They were first dissolved in dimethylsulfoxide (Sigma) to a concentration of 10 mM and then diluted with poly(vinyl alcohol) solution (PVA, 1 wt% in water, MW ca. 13000–23000; Sigma) to ca. 10 μM. Sample (10 μL) was dropped onto the uniaxial wrinkles (50 nm thick gold) and a glass plate and then spin-coated at 3000 rpm for 2 min to form a sample layer with tens of nanometers thickness [33]. PVA polymers are used to form a buffer layer between the metal surface and fluorophores to avoid metal-induced quenching by direct contact [33]. The fluorescence images were acquired using a wide-field epifluorescence microscope (TE 2000-U; Nikon) equipped with a illumination system (X-Cite Series 120; EXFO) and a green color excitation filter (D540/25X; Chroma Tech). The emission was collected by a 40×, numerical aperture (NA) 0.75 objective (Plan Fluor; Nikon) with a 590–650 nm band-pass filter (D620/60 M; Chroma Tech) and recorded with a charge-coupled device (CoolSNAP EZ; Photometrics). For fluorescence lifetime measurement, samples were mounted on a homemade confocal optical microscope for inspection. Excitation of the samples was performed through a 100×, NA 0.7 objective (Nikon) using a frequency-doubled mode-locked ultrafast Ti:Sapphire laser (MIRA 900; Coherent) operating at 410 nm with a 76 MHz repetition rate. Emission passing through a 410 nm notch filter (CVI) and a 590–650 nm band-pass filter (D620/60 M; Chroma Tech) was detected by an avalanche photodiode (PDM 50ct; MPD). The corresponding fluorescence decays were measured with a time-correlated single-photon counting module (PH300; Picoquant).

[1] K. Efimenko, M. Rackaitis, E. Manias, A. Vaziri, L. Mahadevan, J. Genzer, *Nat. Mater.* **2005**, *4*, 293.

[2] E. Cerda, K. Ravi-Chandar, L. Mahadevan, *Nature* **2002**, *419*, 579.

[3] Z. Huang, W. Hong, Z. Suo, *Phys. Rev. E* **2004**, *70*, 030601.

[4] J. Y. Chung, A. J. Nolte, C. M. Stafford, *Adv. Mater.* **2009**, *21*, 1356.

[5] E. Rebollar, I. Frischauf, M. Olbrich, T. Peterbauer, S. Hering, J. Preiner, P. Hinterdorfer, C. Romanin, J. Heitz, *Biomaterials* **2008**, *29*, 1796.

[6] X. F. Wang, C. A. Ohlin, Q. H. Lu, J. Hu, *Biomaterials* **2008**, *29*, 2049.

[7] H. Q. Jiang, D. Y. Khang, J. Z. Song, Y. G. Sun, Y. G. Huang, J. A. Rogers, *Proc. Natl. Acad. Sci. USA* **2007**, *104*, 15607.

[8] D. H. Kim, J. H. Ahn, W. M. Choi, H. S. Kim, T. H. Kim, J. Z. Song, Y. G. Y. Huang, Z. J. Liu, C. Lu, J. A. Rogers, *Science* **2008**, *320*, 507.

[9] N. Bowden, S. Brittain, A. G. Evans, J. W. Hutchinson, G. M. Whitesides, *Nature* **1998**, *393*, 146.

[10] M. G. Urdaneta, R. Delille, E. Smela, *Adv. Mater.* **2007**, *19*, 2629.

[11] S. P. Lacour, S. Wagner, Z. Y. Huang, Z. Suo, *Appl. Phys. Lett.* **2003**, *82*, 2404.

[12] C. M. Stafford, C. Harrison, K. L. Beers, A. Karim, E. J. Amis, M. R. Vanlandingham, H. C. Kim, W. Volksen, R. D. Miller, E. E. Simonyi, *Nat. Mater.* **2004**, *3*, 545.

[13] H. D. Rowland, W. P. King, J. B. Pethica, G. L. Cross, *Science* **2008**, *322*, 720.

[14] F. Yang, E. Wornyo, K. Gall, W. P. King, *Nanotechnology* **2007**, *18*, 285302.

[15] W. T. S. Huck, N. Bowden, P. Onck, T. Pardoen, J. W. Hutchinson, G. M. Whitesides, *Langmuir* **2000**, *16*, 3497.

[16] M. Watanabe, T. Hirai, *J. Polym. Sci, Part B: Polym. Phys.* **2004**, *42*, 2460.

[17] P. J. Yoo, K. Y. Suh, S. Y. Park, H. H. Lee, *Adv. Mater.* **2002**, *14*, 1383.

[18] M. Long, M. A. Sprague, A. Grimes, B. D. Rich, M. Khine, *Appl. Phys. Lett.* **2009**, *94*, 133501.

[19] A. Grimes, D. N. Breslauer, M. Long, J. Pegan, L. P. Lee, M. Khine, *Lab Chip* **2008**, *8*, 170.

[20] C. S. Chen, D. N. Breslauer, J. I. Luna, A. Grimes, W. C. Chin, L. P. Lee, M. Khine, *Lab Chip* **2008**, *8*, 622.

[21] J. Genzer, J. Groenewold, *Soft Matter* **2006**, *2*, 310.

[22] J. Groenewold, *Physica A* **2001**, *298*, 32.

[23] B. Wu, A. Heidelberg, J. J. Boland, *Nat. Mater.* **2005**, *4*, 525.

[24] J. H. Zhao, M. Kiene, C. Hu, P. S. Ho, *Appl. Phys. Lett.* **2000**, *77*, 2843.

[25] M. D. Uchic, D. M. Dimiduk, J. N. Florando, W. D. Nix, *Science* **2004**, *305*, 986.

[26] F. Avilés, L. Llanes, A. I. Oliva, *J. Mater. Sci.* **2009**, *44*, 2590.

[27] J. R. Lakowicz, K. Ray, M. Chowdhury, H. Szmacinski, Y. Fu, J. Zhang, K. Nowaczyk, *Analyst* **2008**, *133*, 1308.

[28] J. Malicka, I. Gryczynski, J. R. Lakowicz, *Biochem. Biophys. Res. Commun.* **2003**, *306*, 213.

[29] E. G. Matveeva, Z. Gryczynski, J. R. Lakowicz, *J. Immunol. Methods* **2005**, *302*, 26.

[30] J. Zhang, J. R. Lakowicz, *Opt. Express* **2007**, *15*, 2598.

[31] I. Abdulhalim, A. Karabchevsky, C. Patzig, B. Rauschenbach, B. Fuhrmann, E. Eltzov, R. Marks, J. Xu, F. Zhang, A. Lakhtakia, *Appl. Phys. Lett.* **2009**, *94*, 063106.

[32] K. Matsuda, Y. Ito, Y. Kanemitsu, *Appl. Phys. Lett.* **2008**, *92*, 211911.

[33] K. Ray, R. Badugu, J. R. Lakowicz, *J. Am. Chem. Soc.* **2006**, *128*, 8998.

[34] J. Zhang, Y. Fu, M. H. Chowdhury, J. R. Lakowicz, *Nano Lett.* **2007**, *7*, 2101.

[35] M. Bally, M. Halter, J. Voros, H. M. Grandin, *Surf. Interface Anal.* **2006**, *38*, 1442.

[36] S. Chung, J. H. Lee, M. W. Moon, J. Han, R. D. Kamm, *Adv. Mater.* **2008**, *20*, 3011.

[37] K. Kim, D. J. Kim, E. J. Cho, J. S. Suh, Y. M. Huh, D. Kim, *Nanotechnology* **2009**, *20*.